An arbitrary waveform magnetic nanoparticle relaxometer with an asymmetrical three-section gradiometric receive coil

Can Barış TOP[*]

ASELSAN Research Center, ASELSAN A.Ş., Ankara, Turkey

Abstract: Magnetic nanoparticles (MNPs) have a wide range of clinical applications for imaging, therapy, and biosensing. Superparamagnetic MNPs can be directly visualized with high spatiotemporal resolution using the magnetic particle imaging (MPI) modality. The image resolution of MPI depends on the relaxation properties of the MNPs. Therefore, characterization of MNP response under alternating magnetic field excitation is necessary to predict MPI imaging performance and develop optimized MNPs. Biosensing applications also make use of the change in the relaxation response of MNPs after binding to a target agent. As MNP relaxation properties change with temperature and viscosity, noninvasive probing of these microenvironmental properties is possible. In this work, we present an untuned relaxometer to measure the relaxation properties of the MNPs in a wide frequency and amplitude range. The developed relaxometer can produce above 80 mTpp magnetic field at up to 60 kHz frequency, and above 14 mTpp at up to 150 kHz frequency. An asymmetrical three-section gradiometer receive coil is used to cancel the direct coupled signal from the transmit coil. The position of one of the receive coil sections is manually tuned using a rotating knob for improved decoupling. The tuning coil section has a lower number of turns compared to the other sections to decrease the sensitivity to mechanical movement. By tuning the knob, the transmit-receive coupling can be decreased below −80 dB. We analyzed the x-space image resolution, harmonic levels, and effect of the number of used harmonics on the resolution for two different commercially available superparamagnetic iron oxide MNPs (Perimag and Synomag-D) in a multifrequency/multiamplitude measurement scheme. The magnetization properties of MNPs for arbitrary waveforms can be measured efficiently using the developed relaxometer.

Key words: Magnetic particle imaging, magnetic nanoparticles, magnetic particle relaxometer, biosensing, magnetic nanoparticle spectrometer

1. Introduction

Superparamagnetic magnetic nanoparticles (MNPs) exhibit distinct properties that make them attractive in a wide range of clinical applications [1]. They have been used as contrast agents in magnetic resonance imaging (MRI) modifying both T1 and T2 contrasts [2]. MNPs can also be used in therapy; they can be heated by an alternating magnetic field (AMF) for inducing hyperthermia, in which the tissue temperature is locally increased [3]. At elevated temperatures, tumor cells are vulnerable, and therefore become more sensitive to chemotherapy or radiotherapy. Controlled drug release is another application area that uses AMF heating of MNPs [4]. The distribution of MNPs can be directly imaged using the magnetic particle imaging (MPI)

[*]Correspondence: cbtop@aselsan.com.tr

method [5, 6]. MPI has opened new horizons for clinical use of the MNPs. Angiography, interventional radiology, tumor imaging, cell tracking, diffusion imaging, temperature, and viscosity probing are some of the proposed clinical applications of MPI [1, 5–13].

An MPI system uses an inhomogeneous magnetic field, in which there is a low field region (the field free region, FFR) and a high field region. The MNPs inside the FFR can align their magnetization to an additional magnetic field, while the MNPs outside this region are magnetically saturated. The additional magnetic field is generally applied as a homogeneous time-varying field (called the drive field, DF) to the whole imaging field of view (FOV). The response of the MNPs in the FFR is sensed generally using an inductive receive coil. By scanning the FFR inside the FOV, the distribution of the MNPs can be reconstructed. The inhomogeneous magnetic field is called the selection field (SF), since it selects the position where the MNPs are responsive.

The resolution of the MPI images depends on both magnetic field properties (gradient of the SF; amplitude and frequency of the DF) and MNP magnetization properties. The magnetization vectors of the MNPs react to an externally applied magnetic field by Néel and Brownian relaxation mechanisms. Néel relaxation is the change of magnetization direction in the crystal structure of the MNP without physical rotation [14, 15], while Brownian relaxation is the change of direction of the magnetization vector by the physical rotation of the MNP [16]. As the relaxation time depends on MNP temperature and ambient viscosity, probing temperature and viscosity of the microenvironment is possible by measuring relaxation response of the MNPs [9–12]. Molecular binding of antibody-coated MNPs affects Brownian relaxation time, which can be used to detect specific targets such as tumors, bacteria, and viruses [13].

Measurement of the magnetization response of MNPs to an applied DF is not only useful for characterizing the MNP signal (measuring the dependence of magnetic relaxation on the environmental conditions and determining the received frequency spectra and MPI image resolution), but also for monitoring the MNP synthesis process, as well [17]. Both narrowband single or multifrequency [17–22] and wideband [23] relaxometer/spectrometer systems have been proposed for the measurement of MNP relaxation properties for MPI. These systems generally use a DF in a single direction and record the response of the MNPs to the applied drive field. 2D and 3D relaxometers have also been proposed to emulate complex excitations for MPI [24, 25]. Narrowband relaxometer systems can have a large measurement volume capacity, but they require a matching circuit to compensate for the large inductance of the transmit coil. On the other hand, wideband systems use a transmit coil with a low inductance value, so there is no need for a matching circuit. Consequently, the effect of arbitrary waveforms on the particle signal can be analyzed, and automated multifrequency/multiamplitude measurements are possible in a small amount of time. In [23], a wideband relaxometer was presented, which uses a two-section gradiometer receive coil to decouple the transmit coil signal from the MNP response. To minimize the coupled signal, one of the gradiometer coils is mechanically moved with a high-precision shimming mechanism.

In this study, we present a wideband relaxometer structure that can operate in the DC 200-kHz frequency range. We use a three-section gradiometer receive coil, which can be tuned to decouple the transmit signal by manually turning a cylindrical knob. The rotation of the knob moves the third (lower) coil section up and down. The third section has a smaller number of turns than the other sections so that the sensitivity to knob rotation is decreased. This allows for manual fine tuning without using precision instrumentation. We measured the response of two types of MNPs, Perimag and Synomag-D (Micromod Partikeltechnologie GmbH, Germany), for 3 mT, 5 mT, and 7 mT sinusoidal DF amplitude in the 1–149 kHz frequency range. We also analyzed the

point spread function (PSF) for x-space MPI image reconstruction using a sinusoidal DF added to a triangular pulse. Furthermore, we analyzed the effect of number of included harmonics on the PSF.

2. Methods

2.1. Transmit and receive coil design

The transmit (or drive) field is generated using an 18-turn single layer solenoidal coil with 27 mm length, 12 mm diameter, and 1.2 mm thickness. A 200-strand $\times 71$ μm Litz wire (PACK Rupalit V155, Rudolf Pack GmbH and Co., Germany) was used for the coil construction. The transmit coil generates 0.7 mT/A magnetic field in the sensitive region. The magnetic field has 95% homogeneity within a 12 mm region along the coil axis. The inductance of the coil was measured as 3.1 μH at 1 kHz frequency with an E4980AL (Keysight Tech., USA) LCR meter. The coil self-resonance frequency was above 1 MHz.

The receive coil consists of three 9 mm-diameter solenoidal single layer sections with 17, 20, and 5 turns and 0.5 mm thickness. The 5-turn coil section is designed to move along the coil axis. The number of turns of the moving coil is kept smaller than the other sections so that the sensitivity to movement is reduced, and the decoupling can be finely adjusted. The middle section is sensitive to the magnetization of the MNPs, while the top and bottom sections (winded in the reverse direction) are used to suppress the coupled transmit signal (Figure 1). The receive coil has a maximum sensitivity of 1.7 mT/A. The sensitivity is halved at ± 3 mm distance from the middle coil center. The mechanical design of the relaxometer allows positioning of a 0.2 mL PCR sample tube in the center region. Coil diameters are minimized to increase their sensitivity to the MNP signal. The receive coil was produced using a PACK Rupalit V155 20-strand $\times 32$ μm Litz wire. The measured receive coil inductance was 7 μH, and the coil self-resonance frequency was above 1 MHz. The placement of transmit and receive coils and the MNP sample tube are shown in Figure 1a.

2.2. Mechanical design

The mechanical housing was designed such that the bottom receive coil section can be moved up and down manually using a turning knob with 18 mm diameter. The bottom receive coil section was wound on a movable part housing a nut (Figures 1b and 1c). At the bottom side, a screw was the attached to a rotating knob. When the knob is rotated, the rotation of the screw moves the nut and attached movable part (1.4 μm per degree). The bottom coil can be moved in a total range of 12 mm. The mechanical housing was produced using Delrin material.

2.3. Relaxometer setup

The relaxometer measurement setup is shown in Figure 2a. The transmit signal is generated using a computer controlled waveform generator (Keysight 33500B) and amplified using an AE Techron 7224 Power Amplifier (AETechron Inc., USA). The MNP signal induced in the receiving coil is amplified with an SR 560 (Stanford Research Systems, USA) preamplifier and digitized using an NI 6363 USB (National Instruments, USA) analog-digital converter (2 MS/s). A current probe (Keysight 1146B) and an oscilloscope (Keysight DSO1014A) are used to monitor the transmit coil current. The maximum current value that can be applied to the transmit coil at different frequencies was measured to determine the frequency-dependent amplitude limitations (Figure 2b). In these measurements, we limited the current such that the maximum field does not exceed 80 mTpp.
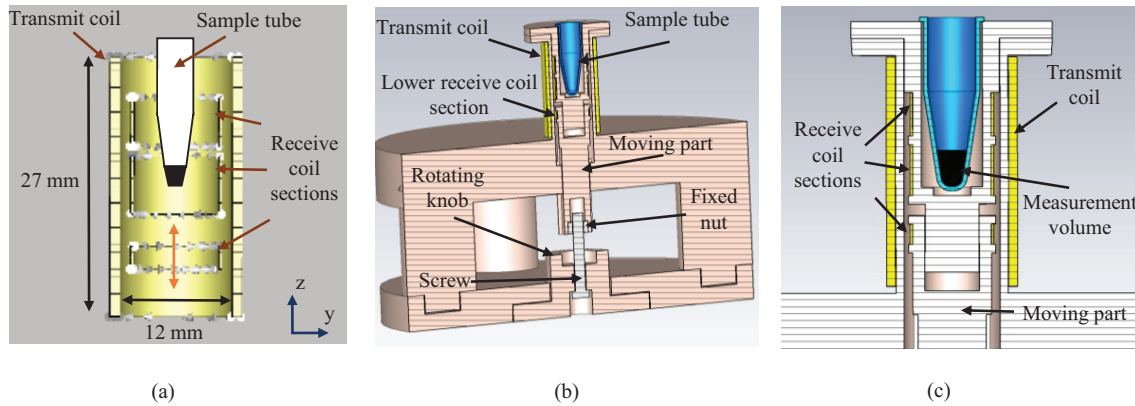
Figure 1. a) Transmit and receive coil geometry. The receive coil is designed as a gradiometer with three sections. The winding directions of the coils are shown as silver arrows. The lowest section can be moved in the z-direction for fine decoupling. b) Cross-section view of the relaxometer showing the moving coil section and the rotating knob. c) Zoomed-in cross-section of the measurement chamber.
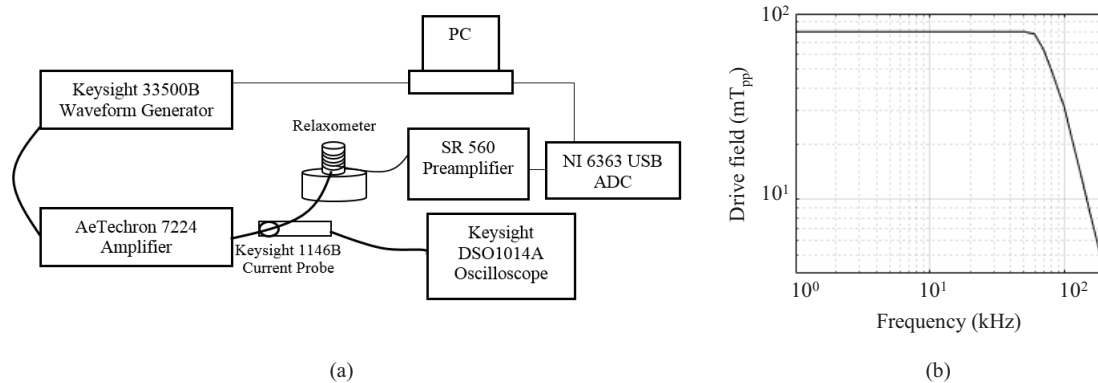

Figure 2. a) Relaxometer measurement setup, b) peak-to-peak magnetic field amplitude limits of the relaxometer as a function of frequency.

We measured the coupling between the transmit and receive coils at 25 kHz frequency and 1 mT drive field amplitude as a function of rotating knob angle (10 measurements at each knob position). By adjusting the knob angle, the coupling was decreased down to −95 dB compared to the case where only the middle receive coil section is present (Figure 3a). Nevertheless, at this coupling level, the received signal was sensitive to the vibration caused by the sample tube insertion and removal process. The coupled signal level was consistent (not affected by sample placement) at the knob position for −83 dB coupling level.

2.4. MNP measurements

Two different MNPs, Perimag and Synomag-D (Micromod Partikeltechnologie GmbH, Germany) were measured using the developed relaxometer. Perimag is a dextran-coated iron oxide MNP with 19 nm average core size and 130 nm hydrodynamic diameter [26]. Synomag-D is a nanoflower shaped iron oxide core dextran-coated nanoparticle [27]. We used 70 nm hydrodynamic sized Synomag-D particles in this study.

Two types of waveforms were used in the experiments. In the first one, a sinusoidal drive field waveform was applied at 3 mT, 5 mT, and 7 mT amplitudes, and the frequency was swept between 1 kHz and 149 kHz in

2 kHz steps automatically. A 40-loop sine wave was applied for each measurement and averaged 10 times. The first and last five cycles were excluded, and the remaining 30 cycles were averaged. Before MNP measurements, the coupled signal was measured and adjusted to a stable minimum value using the tuning knob. A background measurement was taken before the MNP measurements and subtracted from the latter to obtain the MNP magnetization response. The signal was transformed to the frequency domain using the fft function of MATLAB (MathWorks, USA) to analyze the harmonics of the MNP signal. The harmonics are a result of the nonlinear magnetization curve of the MNPs. High harmonic levels indicate that the MNP has a sharp saturation curve, suggesting high MPI resolution. Harmonic levels of Perimag and Synomag-D iron oxide MNPs were compared as a function of drive frequency and amplitude. The received signal spectrum with and without Perimag nanoparticles is given in Figure 3b for 5 mT drive field amplitude at 25 kHz frequency.
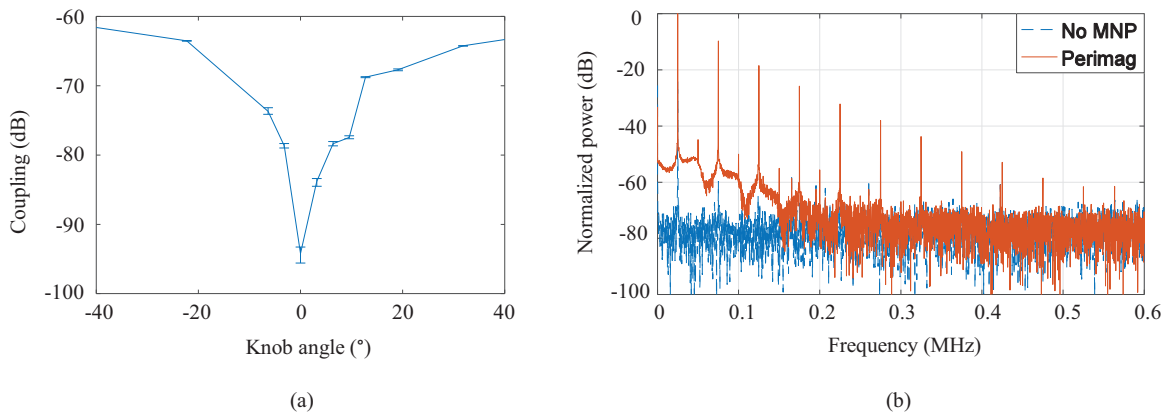

(a)
(b)

Figure 3. a) Measured coupling as a function of rotation angle of the tuning knob. The error bars represent the minimum and maximum values of 10 measurements. b) Received signal power as a function of frequency with and without Perimag nanoparticles.

In the second waveform, a low amplitude sinusoidal signal was added on top of a high amplitude single cycle 10 ms triangular wave (Figure 4a). This waveform was used to determine the PSF of the MNPs for x-space MPI reconstruction. The received signal for this waveform is shown in Figure 4b. In the initial experiments, the effect of the applied field amplitude on the full width at half maximum resolution (FWHM) was analyzed. A 25 kHz frequency and 5 mT peak amplitude drive field was added to a triangular wave with amplitude ranging between 15 mT to 30 mT in 5 mT steps. Then the frequency of the drive field was swept between 1 kHz and 149 kHz in 2 kHz steps for 20 mT peak applied field level. The measurements were repeated for 3 mT, 5 mT, and 7 mT sinusoidal drive field amplitude. Relatively small amplitude levels were used in the experiments for the following reasons: First, the drive field amplitude is limited by peripheral nerve stimulation limits, which was shown to be below 7 mT at 25 kHz frequency for a human torso [28]. Second, the resolution of MPI images increases with decreasing drive field amplitude [29]. Using this waveform, we analyzed the effect of drive field frequency and amplitude on the x-space image resolution. We also analyzed how the resolution changes as a function of number of harmonics included in the reconstruction process.

In all measurements, a 20 μL undiluted MNP sample was used. The received data were normalized by the iron content of the samples. Measurements were made at room temperature.
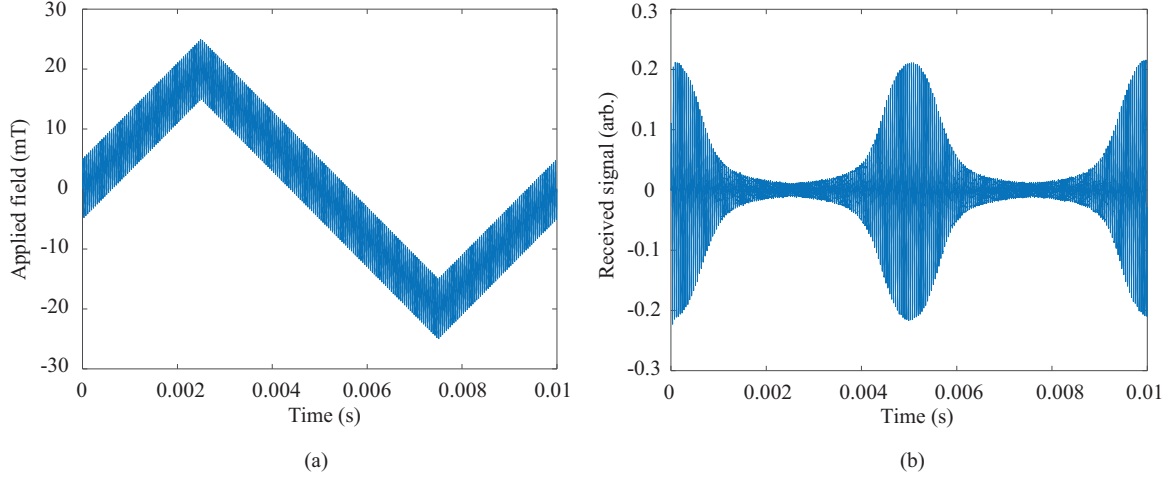
Figure 4. (a) Waveform used for the point spread function measurements. Sinusoidal drive field is added to a triangular pulse. (b) Received signal for the sine added triangular waveform. The nanoparticles partially saturate in the high drive field region, while the signal level is maximum around the zeros of the triangular pulse.

2.5. Received signal processing for MNP parameter extraction

The induced voltage in the receive coil due to the magnetization on MNPs can be written as follows [6]:

$$s(t) = -\frac{d}{dt} \int_V \mathbf{B_r}(\mathbf{r}) \cdot \mathbf{M}(\mathbf{r}, t) d\mathbf{r}, \tag{1}$$

where $\mathbf{M}(\mathbf{r}, t)$ is the total magnetization of the MNPs inside the sensing volume V, and $\mathbf{B_r}(\mathbf{r})$ is the receive coil sensitivity in (T/A). The magnetization response of the MNPs is described by the Langevin function $\mathcal{L}[\cdot]$ and a relaxation term depending on particle, drive field, and environmental properties [6]. The relaxometer signal can be obtained using (1) and the magnetization response of the MNPs [6]. Assuming a homogeneous z-directed drive field and receive coil sensitivity, the received signal can be written as:

$$s(t) = (-B_r m V \beta \rho \dot{\mathcal{L}}(\beta H(t)) \dot{H}(t)) * r(t), \tag{2}$$

where m is the particle magnetic moment, ρ is the iron concentration, V is the total sensing volume, β is a factor depending on the saturation magnetization of the particles, and $H(t)$ is the drive magnetic field. Dots over the Langevin function and the drive field refer to the time derivative operation. $r(t)$ is the relaxation term, which can be modeled by the Debye relaxation process [30].

The PSF of the model based on x-space MPI reconstruction [31] can be analyzed on the time domain signal using (2) [29]. The received signal $s(t)$ involves a multiplication with the time derivative of the drive field (which also corresponds to the velocity of the field free point in MPI). To remove this effect, the received signal should be divided by $\dot{H}(t)$. Since the received signal to noise ratio is degraded around zero crossings of the velocity, a thresholding operation is performed, and only the portions of the $s(t)$ at which $\frac{\dot{H}(t)}{max(||\dot{H}(t)||)}$ is greater than a threshold ξ is preserved. Then the remaining signal sections are interpolated on a drive field grid, and overlapping sections of the drive field cycles are averaged [32]. In the last stage the PSF is normalized, and the FWHM value is obtained. In this study, we used a threshold of $\xi = 0.8$. The resultant signal sections

were interpolated on a –22 mT to 22 mT grid in 0.01 mT steps. It should be noted that we obtained the native PSF, which involved the effect of nonadiabatic magnetization [30]. The FWHM obtained in mT units can be translated into spatial FWHM in millimeters simply by dividing the FWHM value into the magnetic field gradient (in T/m units) of the selection field [33]. For example, a 5 mT FWHM corresponds to 5 mm spatial FWHM for 1 T/m gradient.

3. Results

The first six odd harmonic amplitudes for the two types of MNPs are given in Figure 5 as functions of frequency for different drive field amplitude levels. As a result of the inductive measurement, the received signal amplitudes increase with frequency. The received signal amplitude also increases with drive field amplitude, as expected. This increase is more pronounced for higher harmonics as a result of the nonlinear magnetization curve of the magnetic nanoparticles. The results show that the Synomag-D has a higher first harmonic level compared to Perimag MNPs. On the other hand, Perimag nanoparticles exhibit higher levels of higher harmonics relative to the first harmonic.
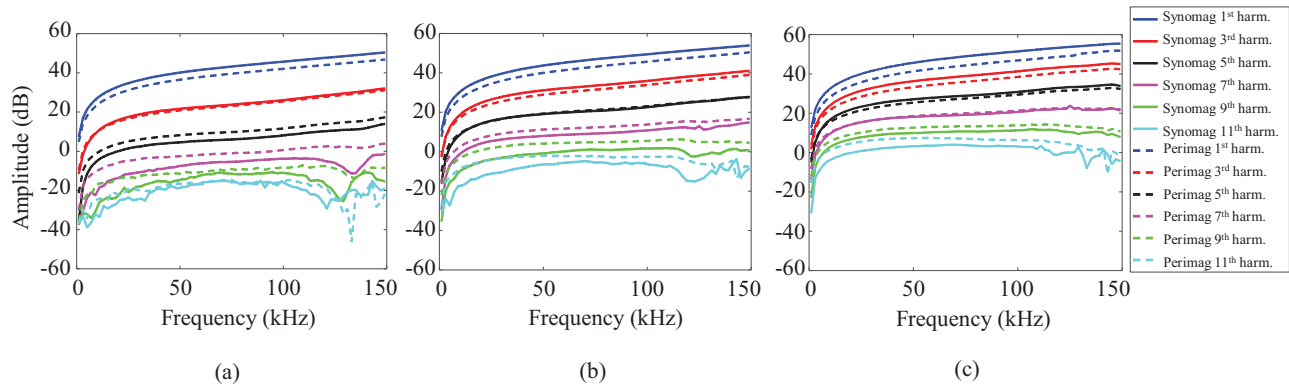

Figure 5. Received harmonic levels (dB) of Synomag-D and Perimag nanoparticles as a function of frequency at (a) 3 mT, (b) 5 mT, and (c) 7 mT transmit fields. The measurements are normalized with iron concentration.

The PSF of the MNPs for 5 mT drive field amplitude at 25 kHz frequency are given in Figure 6a in mT units. The odd harmonic levels normalized to the first harmonic are also given for the same excitation parameters (Figure 6b). Consistent with the results of the harmonic levels, Perimag MNPs exhibit higher resolution compared to Synomag-D nanoparticles. The PSF of Perimag MNPs for different peak values of the triangular pulse (at 25 kHz and 5 mT sinusoidal drive field) are shown in Figure 6c. As can be seen in the figure, the change in FWHM values is not significant (5.52 $\pm$ 0.04 mT), showing that driving the MNPs to full saturation is not necessary to predict the x-space FWHM.

The effect of number of used harmonics on the FWHM is shown in Figure 7. The results show that as the number of used harmonics increases, the effect of the DF amplitude on the resolution decreases. For small DF amplitude levels, the FWHM converges faster to its final value. The results also show that small DF amplitude levels result in higher resolution compared to large DF amplitude levels, which is consistent with previous studies [23, 29].

The FWHM values of the MNPs with respect to frequency are given in Figure 8 for different DF amplitude levels. The first 11 harmonics were included in is calculation. Perimag MNPs exhibit higher resolution compared to Synomag-D MNPs. The effect of DF amplitude is also more pronounced for Perimag nanoparticles. The
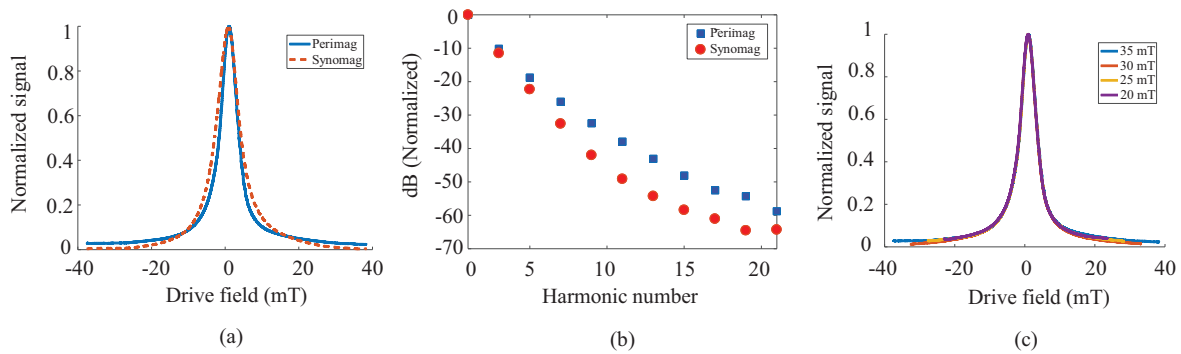
Figure 6. (a) The PSF of the Perimag and Synomag-D nanoparticles for 5 mT drive field amplitude at 25 kHz. (b) Normalized odd harmonic levels (dB) of Perimag and Synamag-D nanoparticles for 5 mT peak drive field at 25 kHz. (c) The PSF of Perimag nanoparticles for different peak applied fields between 20 mT to 35 mT. The drive field frequency and amplitude are 25 kHz and 5 mT, respectively.
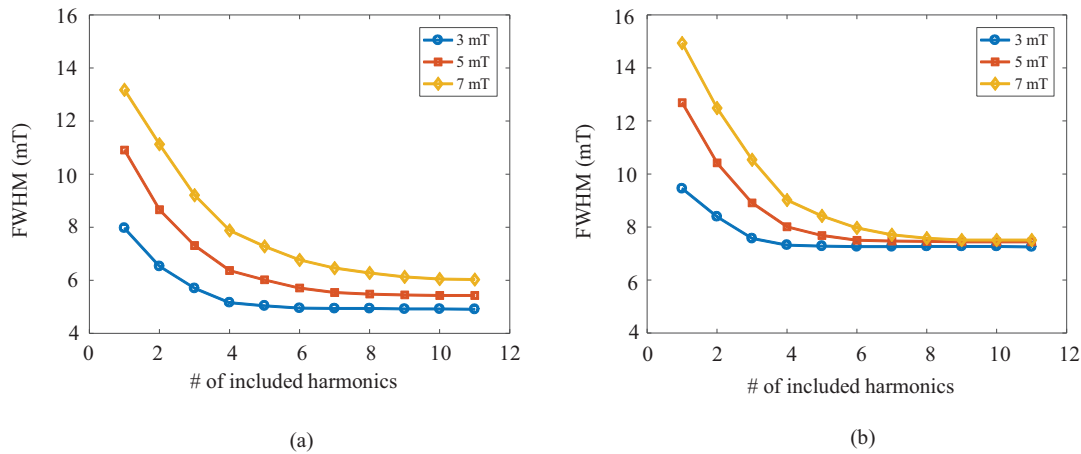

Figure 7. (a) The effect of number of harmonics used on the FWHM of the PSF for (a) Perimag and (b) Synomag-D nanoparticles at 25 kHz drive field frequency.

resolution decreases monotonically with frequency after about 15 kHz for Perimag nanoparticles. For Synomag-D nanoparticles, the resolution improves up to about 20 kHz frequency, then decreases monotonically.

4. Discussion

The developed relaxometer covers a wide frequency and amplitude parameter range used in MPI, considering safety limitations. Higher fields are possible with increased transmit power. We have shown that the transmit signal can be isolated efficiently with the proposed coil arrangement using a simple mechanical construction. Since the fundamental frequency is retained in the current relaxometer, there is no need to overlap the drive field cycles for DC recovery [29]. In addition, untuned design allows the use of arbitrary waveforms.

The use of gradiometric coils is a common practice to decrease the direct coupled signal [20–23, 34, 35]. Nevertheless, the decoupling level may not be sufficient enough to decrease the coupled transmit signal below the nanoparticle response [35]. The reported coupling values for some of the gradiometer designs are between –45 dB and –67 dB [23, 34, 35]. Addition of an active decoupling mechanism was proposed in [35] to further increase
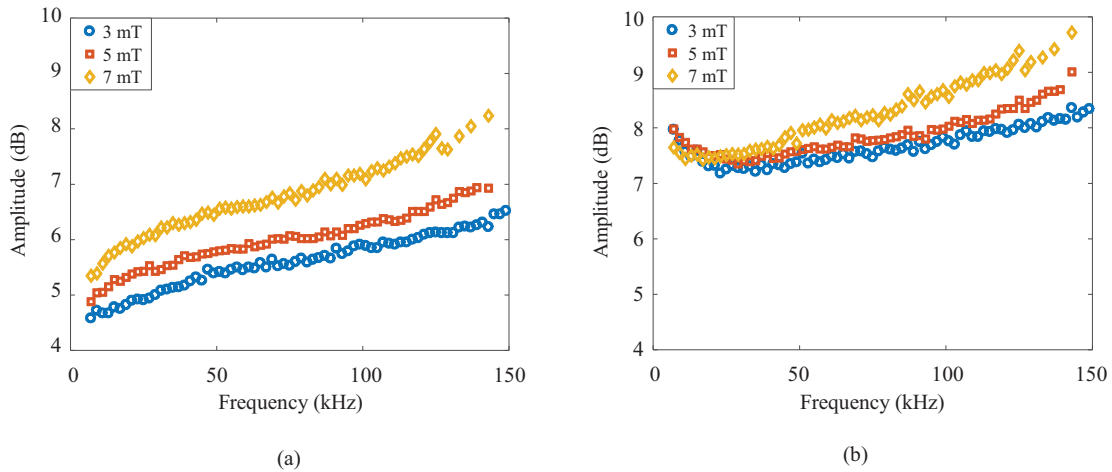
Figure 8. The FWHM of MNPs as a function of frequency for (a) Perimag and (b) Synomag-D nanoparticles.

the decoupling between transmit and receive coils. Our design achieved a high degree of decoupling down to -95 dB, thanks to the asymmetrical three-section gradiometer tuning mechanism that decreases sensitivity to mechanical motion.

The FWHMs calculated using an x-space-based reconstruction scheme suggest that the Perimag nanoparticles exhibit higher resolution compared to the Synomag-D nanoparticles. On the other hand, the signal level of the Synomag-D nanoparticles normalized by the iron content was higher than that of Perimag nanoparticles. Consistent with the previous studies, the resolution increased with decreasing DF amplitude and frequency in general, except for the Synomag-D nanoparticles below 20 kHz DF frequency.

In this study, we also analyzed the FWHM resolution as a function of number of used harmonics, which may be informative for MPI drive waveform parameter selection. The results showed that for lower DF amplitude levels, FWHM converges faster in terms of number of harmonics used in the reconstruction. Our results also imply that if a sufficient number of harmonics is used, high DF amplitudes can result in similar resolution with low DF amplitudes. This was specifically observed for Synomag-D nanoparticles, suggesting that a high drive field is advantageous in terms of resolution and SNR. On the other hand, low DF amplitude still resulted in better resolution for Perimag nanoparticles. In general, drive field amplitude should be optimized for each type of nanoparticle.

5. Conclusions

We have developed a relaxometer for MNP characterization enabling the use of arbitrary waveforms. The drive coil has a small inductance so that a matching circuit is not required and wideband operation is possible. The drive coil and the manually movable section of the gradiometric receive coil has a small mutual inductance. In this way, the sensitivity to movement is decreased and a high transmit to receive decoupling is provided with a simple mechanical construction. The relaxometer was used to characterize two types of iron oxide MNPs, showing its efficiency for arbitrary drive field waveforms.

1352

Acknowledgment

References

[1] Panagiotopoulos N, Duschka RL, Ahlborg M, Bringout G, Debbeler C et al. Magnetic particle imaging: current developments and future directions. International Journal of Nanomedicine 2015; 10: 3097–3114. doi: 10.2147/IJN.S70488

[2] Stephen ZR, Kievit FM, Zhang M. Magnetite nanoparticles for medical MR imaging. Materials Today 2011; 14(7–8): 330–338. doi: 10.1016/S1369-7021(11)70163-8

[3] Giustini AJ, Petryk AA, Cassim SM, Tate JA, Baker I et al. Magnetic nanoparticle hyperthermia in cancer treatment. Nano LIFE 2010; 1: 01n02. doi:10.1142/S1793984410000067 .

[4] Mura S, Nicolas J, Couvreur P. Stimuli-responsive nanocarriers for drug delivery. Nature Materials 2013; 12 (11): 991–1003. doi: 10.1038/nmat3776

[5] Gleich B, Weizenecker J. Tomographic imaging using the nonlinear response of magnetic particles. Nature 2005; 435 (7046): 1214–1217. doi: 10.1038/nature03808

[6] Knopp T, Buzug TM. Magnetic Particle Imaging: An Introduction to Imaging Principles and Scanner Instrumentation. Heidelberg, Germany: Springer-Verlag, 2012.

[7] Borgert J, Schmidt JD, Schmale I, Rahmer J, Bontus C et al. Fundamentals and applications of magnetic particle imaging. Journal of Cardiovascular Computed Tomography 2012; 6 (3): 149–153. doi: 10.1016/j.jcct.2012.04.007

[8] Knopp T, Gdaniek N, Möddel M. Magnetic particle imaging: from proof of principle to preclinical applications. Physics in Medicine and Biology 2017; 62 (14): R124. doi: 10.1088/1361-6560/aa6c99

[9] Weaver JB. The use of magnetic nanoparticles in thermal therapy monitoring and screening: localization and imaging (invited). Journal of Applied Physics 2012: 111 (7): 07B317. doi: 10.1063/1.3675994

[10] Weaver JB, Rauwerdink AM, Hansen EW. Magnetic nanoparticle temperature estimation. Medical Physics 2009; 36 (5): 1822–1829. doi: 10.1118/1.3106342

[11] Rauwerdink AM, Weaver JB. Viscous effects on nanoparticle magnetization harmonics. Journal of Magnetism and Magnetic Materials 2010; 322 (6): 609–613. doi: 10.1016/j.jmmm.2009.10.024

[12] Utkur M, Muslu Y, Saritas EU. Relaxation-based viscosity mapping for magnetic particle imaging. Physics in Medicine and Biology 2017; 62 (9): 3422–3439. doi: 10.1088/1361-6560/62/9/3422

[13] Rauwerdink AM, Weaver JB. Measurement of molecular binding using the Brownian motion of magnetic nanoparticle probes. Applied Physics Letters 2010; 96 (3): 033702. doi: 10.1063/1.3291063

[14] Néel L. Thermoremanent magnetization of fine powders. Reviews of Modern Physics 1953; 25 (1): 293–295. doi: 10.1103/RevModPhys.25.293

[15] Brown WF. Thermal fluctuations of a single-domain particle. Journal of Applied Physics 1963; 34 (4): 1319–1320. doi: 10.1063/1.1729489

[16] Coffey WT, Cregg PJ, Kalmykov YUP. On the theory of Debye and Néel relaxation of single domain ferromagnetic particles. Advances in Chemical Physics 2007; 1: 263–464. doi: 10.1002/9780470141410.ch5

[17] Malhotra A, von Gladiss A, Behrends A, Friedrich T, Neumann A et al. Tracking the growth of superparamagnetic nanoparticles with an in-situ magnetic particle spectrometer (INSPECT). Scientific Reports 2019; 9 (1): 1–13. doi: 10.1038/s41598-019-46882-6

[18] Biederer S, Sattel T, Knopp T, Lüdtke-Buzug K, Gleich B et al. A spectrometer for magnetic particle imaging. In: Vander Sloten J, Verdonck P, Nyssen M, Haueisen J (editors). 4th European Conference of the International Federation for Medical and Biological Engineering. Berlin, Germany: Springer, 2009, pp. 2313–2316.

[19] Wawrzik T, Schilling M, Ludwig F. Perspectives of magnetic particle spectroscopy for magnetic nanoparticle characterization. In: Buzug TM, Borgert J (editors). Magnetic Particle Imaging. Berlin, Germany: Springer, 2012, pp. 41–45.

[20] Goodwill PW, Tamrazian A, Croft LR, Lu CD, Johnson EM et al. Ferrohydrodynamic relaxometry for magnetic particle imaging. Applied Physics Letters 2011; 98 (26): 262502. doi: 10.1063/1.3604009

[21] Utkur M, Saritas EU. Comparison of different coil topologies for an MPI relaxometer. In: IWMPI 2015 International Workshop on Magnetic Particle Imaging; Istanbul, Turkey; 2015. pp. 1-13. doi: 10.1109/IWMPI.2015.7107082

[22] Behrends A, Graeser M, Buzug TM. Introducing a frequency-tunable magnetic particle spectrometer. Current Directions in Biomedical Engineering 2015; 1 (1): 249–253. doi: 10.1515/cdbme-2015-0062

[23] Tay ZW, Goodwill PW, Hensley DW, Taylor LA, Zheng B et al. A high-throughput, arbitrary-waveform, MPI spectrometer and relaxometer for comprehensive magnetic particle optimization and characterization. Scientific Reports 2016; 6: 1-11. doi: 10.1038/srep34180

[24] Graeser M, Gladiss AV, Weber M, Buzug TM. Two dimensional magnetic particle spectrometry. Physics in Medicine and Biology 2017; 62 (9): 3378–3391. doi: 10.1088/1361-6560/aa5bcd

[25] Chen X, Graeser M, Behrends A, von Gladiss A, Buzug TM. First measurement and SNR results of a 3D magnetic particle spectrometer. International Journal on Magnetic Particle Imaging 2018; 4 (1): 1-20.

[26] Eberbeck D, Dennis CL, Huls NF, Krycka KL, Grüttner C et al. Multicore magnetic nanoparticles for magnetic particle imaging. IEEE Transactions on Magnetics 2013; 49 (1): 269-274. doi: 10.1109/TMAG.2012.2226438

[27] Grüttner C, Kowalski A, Fidler F, Steinke M, Westphal F et al. Synomag nanoflower particles: a new tracer for MPI, physical characterization and initial in vitro toxicity studies. In: IWMPI 2018 International Workshop on Magnetic Particle Imaging; Hamburg, Germany; 2018. pp. 17-8.

[28] Saritas EU, Goodwill PW, Zhang GZ, Conolly SM. Magnetostimulation limits in magnetic particle imaging. IEEE Transactions on Medical Imaging 2013; 32 (9): 1600–1610. doi: 10.1109/TMI.2013.2260764

[29] Croft LR, Goodwill PW, Konkle JJ, Arami H, Price DA et al. Low drive field amplitude for improved image resolution in magnetic particle imaging. Medical Physics 2016; 43 (1): 424–435. doi: 10.1118/1.4938097

[30] Croft LR, Goodwill PW, Conolly SM. Relaxation in x-space magnetic particle imaging. IEEE Transactions on Medical Imaging 2012; 31 (12): 2335–2342. doi: 10.1109/TMI.2012.2217979

[31] Goodwill PW, Conolly SM. The x-space formulation of the magnetic particle imaging process: 1-D signal, resolution, bandwidth, SNR, SAR, and magnetostimulation. IEEE Transactions on Medical Imaging 2010; 29 (11): 1851–1859. doi: 10.1109/TMI.2010.2052284

[32] Lu K, Goodwill PW, Saritas EU, Zheng B, Conolly SM. Linearity and shift invariance for quantitative magnetic particle imaging. IEEE Transactions on Medical Imaging 2013; 32 (9): 1565–1575. doi: 10.1109/TMI.2013.2257177

[33] Kuhlmann C, Khandhar AP, Ferguson RM, Kemp S, Wawrzik T et al. Drive-field frequency dependent MPI performance of single-core magnetite nanoparticle tracers. IEEE Transactions on Magnetics 2015; 51: 3–6.

[34] Schulz V, Straub M, Mahlke M, Hubertus S, Lammers T et al. A field cancellation signal extraction method for magnetic particle imaging. IEEE Transactions on Magnetics 2015; 51: 1-12.

[35] Pantke D, Holle N, Mogarkar A, Straub M, Schulz V. Multifrequency magnetic particle imaging enabled by a combined passive and active drive field feed-through compensation approach. Medical Physics 2019; 46 (9): 4077-4086.